

Reconstructing Shape and Appearance of Thin Film Objects with Hyper Spectral Sensor

Yoshie Kobayashi¹, Tetsuro Morimoto², Imari Sato³, Yasuhiro Mukaigawa⁴,
and Katsushi Ikeuchi⁵

The University of Tokyo, Tokyo, Japan^{1,5}, Toppan Printing Co. Ltd., Tokyo, Japan²,
National Institute of Informatics, Tokyo, Japan³, Nara Institute of Science and
Technology, Nara, Japan⁴

Abstract. Modeling the shape and appearance of a thin film object has promising applications such as heritage-modeling and industrial inspections. In the same time, such modeling is a frontier of computer vision and contains various challenging issues to be solved. In particular, thin film colors show iridescence along the view and lighting directions and how to acquire and formalize the spectral iridescence for shape estimation. This paper aims to model the shapes and appearances of thin film objects from measured reflectance spectra. Thin film reflectance is represented by the incident angle on the object surface, the refractive index and the film thickness. First, we estimate the incident angle of a surface patch on a thin film based on monotonically increasing peak intensities. Then, we apply a characteristics strip expansion method to the peak intensity for estimating the surface normal of the patch. Based on this shape estimation, we estimate refractive index and film thickness from iridescence variance. We experimentally evaluate the accuracy of the estimated shape and estimated parameters. We also demonstrate to reconstruct appearances based on the shape and parameters.

1 Introduction

Modeling the shape and appearance of real world objects is one of the important research in computer graphics and computer vision fields. Such modeling results are widely used to games, movies and cultural heritage digitization to name a few. Appearances of many objects include several complex reflectance properties such as scattering, absorption, diffraction, refraction and interference. These properties make it difficult to model the shapes and appearances of such objects.

Various objects have interference optical properties, such as laminated materials, soap bubbles and oil films. Interference is one of the most intractable effects since its color varies iridescence along the viewing and lighting directions. Yet, modeling shapes and appearances of these objects with interference effects would be useful for diverse applications in industry, biology, archeology and medicine. For example, realizing the digitization of thin film objects, we can obtain more realistic appearance of new coating products in digital space. Several Japanese art crafts such as Tamamushi Shrine were made of wings of green buprestids with interference.

Considering the iridescence of thin film objects, Iwasaki et al.[1] proposed a rendering method based on physical model. This method manually sets optical parameters such as the refractive index and film thickness. In the optics field, there are several methods for estimating the optical parameters of thin film. Interference spectroscopy[2] and ellipsometry[3] are suitable methods for estimating film thickness, but the refractive index and surface must be known and they handle only a spot measurement. Kitagawa [4][5] proposed an image-based method. Kitagawa used RGB values which change along the film thickness. However, this method needs to know the refractive index. Kobayashi *et. al.* [6] proposed a method for estimating the unknown refractive indexes and film thicknesses by using hyper-spectral images. This method can only be applied to flat surfaces in order to control the incident angle.

This paper proposes a novel method for estimating the shape and appearance of thin film objects by using hyper-spectral images. The color variance of thin film is related to the shape and optical parameters. First, we estimate the incident angles of light on the surface. We focus on the monotonically increasing of the local maximum intensity in the hyper-spectral space, which is caused by interference of reflected light. This local maximum intensity depends on the refractive index of the bottom layer. From the known refractive index and the maximum intensity, we can estimate the incident angles. Second, we estimate the normal from the estimated incident angle by using the characteristic strip expansion method. Finally, we can estimate the optical parameters of thin film such as the refractive index and film thickness by least square minimization between measured reflectance and model reflectance. In our experiments, we confirm that our method theoretically works well. Furthermore, we synthesize the appearance of a thin film object by using estimated parameters and evaluate the accuracy.

We assume that a thin film object consists of the top layer, thin film layer and bottom layer as shown in Fig. 1. We also assume that the top layer is air, the target object is convex, and that the captured image is an orthographic projection of the object; hence, the distance between the object and camera is sufficiently far, and the refractive index of the bottom layer is known. In addition to these, we assume the refractive index is constant along wavelengths.

The rest of this paper is organized as follows. In Section 2, we introduce the methods for acquiring and estimating the shape and BRDF and structural color rendering. In Section 3, we introduce a reflectance model of thin film interference. In Section 4, we describe the method used to estimate the shape and BRDF parameters. In Section 5, we evaluate the proposed method on the basis of simulations and real data and discuss the estimation error in the experiment. In Section 6, we discuss experimental errors. In Section 7, we summarize results.

2 Related Work

In computer vision fields, many methods are proposed for estimating shape, for example the stereo method[7], photometric method[8]. All these methods work well for Lambertian, isotropic, and anisotropic reflectance properties. For

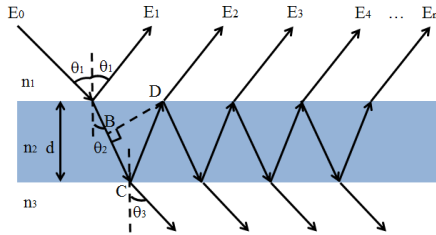


Fig. 1. Schematic diagram of thin film interference when considering multiple reflections. n_1 , n_2 and n_3 are refractive indexes of top layer, thin film and bottom layer respectively. d is film thickness. θ_1 is incident angle. θ_2 is refracting angle. θ_3 is outgoing angle.

more a complicated reflectance property, Morris *et al.*[9] estimate the shape of translucent objects. In an outdoor scene, Oxholm *et al.*[10] estimate the BRDF and shape from a single image under natural illumination. These methods do not consider the iridescence of thin film along the light and view directions. For the optical parameters of reflectance property, Morimoto *et al.* [11] estimated the optical thickness and opacity of layered surfaces, and represented the appearance of layered surfaces of arbitrary thickness. However, this method cannot handle the interference effect of the thin film.

In computer graphics fields, several methods are available for rendering multi-layer interference, diffraction gratings, and refraction. Hirayama *et al.* [12][13] used a multi-layered interference model based on physics and rendered both eyeglass lens and a mother-of-pearl. Modeling the micro-structure of CDs precisely, Sun *et al.* [14][15] were able to render them more realistically. Sadeghi *et al.* [16] calculated refracted ray in vapor by ray tracing and represented an accurate rainbow image that was close to the real one. Cuypers *et al.*[17] showed that the Wigner distribution function can represent the BRDF of diffraction grating as accurately as can a physical model. All these methods are based on physical models and represent the color changes well, but the optical parameters of models must be set manually. Therefore, it is difficult to represent the appearance of a real object without parameters information.

3 Thin-Film Interference Reflectance Model

In the optics fields, a reflectance model of thin film interference[18] was proposed. As shown in Fig. 1, the reflection of thin film consists of only specular reflection. Considering the multi-path reflection in Fig. 1, the observed light E can be

represented by using Eq.(1).

$$\begin{aligned}
E &= E_1 + E_2 + E_3 + E_4 + \dots \\
&= E_0(r_{12} + t_{12}t_{21}r_{23}e^{i\Delta} + t_{12}t_{21}r_{23}^2r_{21}e^{2i\Delta} \\
&\quad + t_{12}t_{21}r_{23}^3r_{21}^2e^{3i\Delta} + \dots) \\
&= E_0(r_{12} + t_{12}t_{21}r_{23}e^{i\Delta}(1 + r_{23}r_{21}e^{i\Delta} \\
&\quad + r_{23}^2r_{21}^2e^{2i\Delta} + \dots)) \\
&= E_0(r_{12} + t_{12}t_{21}r_{23}e^{i\Delta}\frac{1}{1 - r_{23}r_{21}e^{i\Delta}}) \tag{1}
\end{aligned}$$

, where r_{12}, r_{23} and r_{21} are the Fresnel reflection coefficients, and t_{12} and t_{21} are the Fresnel transmittance coefficients. Δ is the phase difference, and represented by Eq. (2). φ is the optical path difference which is the path distance of $BC+CD$ as shown in Fig. 1.

$$\Delta = \frac{2\pi\varphi}{\lambda} \tag{2}$$

$$\varphi = 2dn_2 \cos \theta_2 \tag{3}$$

By setting $r_{21} = -r_{12}$ and $t_{21}t_{12} + r_{12}^2 = 1$, the amplitude of the reflection coefficients is defined as Eq. (4).

$$\begin{aligned}
r &\equiv \frac{E}{E_0} \\
&= r_{12} + t_{12}t_{21}r_{23}e^{i\Delta}\frac{1}{1 - r_{23}r_{21}e^{i\Delta}} \\
&= \frac{r_{12} - r_{12}r_{23}r_{21}e^{i\Delta} + (1 - r_{12}^2)r_{23}e^{i\Delta}}{1 - r_{23}r_{21}e^{i\Delta}} \\
&= \frac{r_{12} + r_{23}e^{i\Delta}}{1 + r_{23}r_{12}e^{i\Delta}} \tag{4}
\end{aligned}$$

The reflectance is given by the square of the absolute value of Eq. (4).

$$R = \left| \frac{r_{12} + r_{23}e^{i\Delta}}{1 + r_{23}r_{12}e^{i\Delta}} \right|^2 \tag{5}$$

Fresnel reflection coefficients in Eq. (4) are defined for the perpendicular (S-wave) and parallel (P-wave) polarizations. r_{12} is defined as Eqs. (6) and (7). r_{23} is defined as Eqs. (8) and (9).

$$r_{12}^s = \frac{n_1 \cos \theta_1 - n_2 \cos \theta_2}{n_1 \cos \theta_1 + n_2 \cos \theta_2} \tag{6}$$

$$r_{12}^p = \frac{n_2 \cos \theta_1 - n_1 \cos \theta_2}{n_2 \cos \theta_1 + n_1 \cos \theta_2} \tag{7}$$

$$r_{23}^s = \frac{n_2 \cos \theta_2 - n_3 \cos \theta_3}{n_2 \cos \theta_2 + n_3 \cos \theta_3} \tag{8}$$

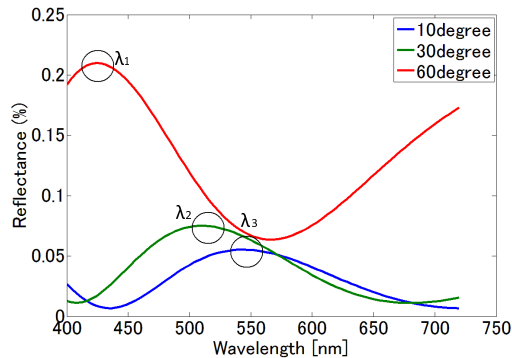


Fig. 2. Reflectance of thin film at 10, 30 and 60 degrees shown as blue, green and red lines respectively. The refractive index of these reflectance is 1.37 and the film thickness is 400 nm.

$$r_{23}^p = \frac{n_3 \cos \theta_2 - n_2 \cos \theta_3}{n_3 \cos \theta_2 + n_2 \cos \theta_3} \quad (9)$$

, where n_1 , n_2 and n_3 are the refractive index of the top layer, thin film and bottom layer respectively. θ_1 is the incident angle. θ_2 is the refracting angle. θ_3 is an angle of outgoing light transmitting the thin film and absorbed by the bottom layer.

With these above equations, Eq. (5) is represented by the incident angle, the refractive index and the film thickness. Eq. (5) describes the reflectance along the incident angle. We use this equation for the BRDF model of the thin film interference.

4 Shape and BRDF Estimation

In this section, we describe a step by step algorithm for estimating the shape and reflectance parameters. First, we estimate the incident angle. Second, we estimate the surface normal from the estimated incident angle by using the characteristic strip expansion method. Finally, we estimate the BRDF parameters, such as refractive index and film thickness, from measured reflectance spectra.

4.1 Incident Angle Estimation

We propose an incident angle estimation method, focusing on the monotonically increasing of the "peak intensity" along the incident angle. Fig. 2 shows an example of the peak intensity and peak wavelength enclosed by circles. The local maximum of the reflectance is caused by the full constructive interference. We call this local maximum reflectance "peak intensity" and the wavelength of this local maximum reflectance "peak wavelength".

We find the peak intensity is only dependent on the refractive index of the ground layer, when it becomes higher than the refractive index of the thin film.

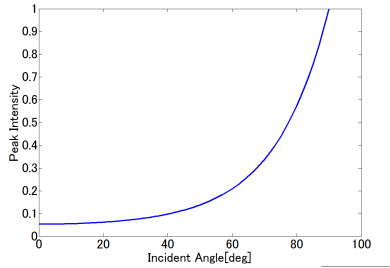


Fig. 3. Peak intensity along incident angle. We calculate intensity with refractive index of the bottom layer of 1.6.

Fig. 3 shows the peak intensity along the incident angle. Using this monotonically increasing intensity, we can estimate the incident angle.

The phase difference (Eq. (2)) becomes 2π at the peak wavelength when the refractive index of the ground layer is higher than that of the thin film[19]. Therefore, $e^{i\Delta}$ becomes 1 at this wavelength, so the reflectance intensity at this wavelength $R(\lambda_t)$ can be determined by Eq. (10).

$$R(\lambda_t) = \left| \frac{r_{12} + r_{23}}{1 + r_{23}r_{12}} \right|^2 \quad (10)$$

, where λ_t is the peak wavelength.

Substituting Eqs. (6) and (8) with Eq. (10), the peak intensity of the perpendicular polarization is defined as Eq. (12).

$$R(\lambda_t) = \left| \frac{\cos \theta_1 - n_3 \cos \theta_3}{\cos \theta_1 + n_3 \cos \theta_3} \right|^2 = \left| \frac{\cos \theta_1 - n_3 \sqrt{1 - \sin^2 \theta_3}}{\cos \theta_1 + n_3 \sqrt{1 - \sin^2 \theta_3}} \right|^2 \quad (11)$$

By Snell's law, $n_1 \sin \theta_1 = n_2 \sin \theta_2 = n_3 \sin \theta_3$ and $n_1 = 1.0$, Eq.(11) becomes as follows.

$$R(\lambda_t) = \left| \frac{\cos \theta_1 - n_3 \sqrt{1 - \frac{1}{n_3^2} \sin^2 \theta_1}}{\cos \theta_1 + n_3 \sqrt{1 - \frac{1}{n_3^2} \sin^2 \theta_1}} \right|^2 = \left| \frac{\cos \theta_1 - \sqrt{n_3^2 - \sin^2 \theta_1}}{\cos \theta_1 + \sqrt{n_3^2 - \sin^2 \theta_1}} \right|^2 \quad (12)$$

The equation shows that the peak intensity of the perpendicular polarization depends on the incident angle and refractive index of the ground layer. In our method, we assume the refractive index of the ground layer is known. We also verified the integral intensity in the whole visible wavelength and found that it becomes monotonic increasing. However, this intensity depends not only on the refractive index of the ground layer but also on the refractive index of the thin film.

We determine the incident angle domain by minimizing the least square error between the peak intensity Eq. (12) and that of the measured reflectance.

$$\text{Arg min}_{\theta_1} |R_o(\lambda_t) - R_m(\lambda_t)|^2 \quad (13)$$

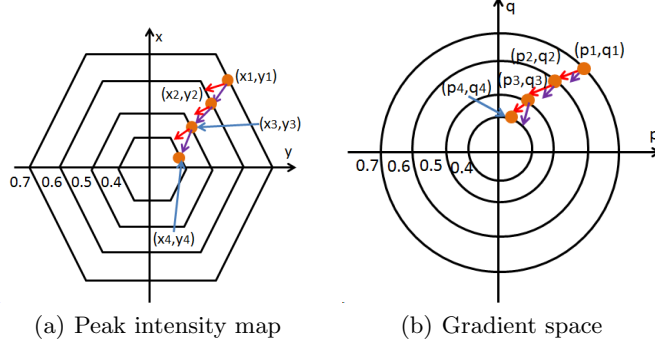


Fig. 4. Example of estimation using the characteristic expansion method. (a) the image which is mapped peak intensity to each pixel. (b) shows contour line in the gradient space.

$R_o(\lambda_t)$ is the measured reflectance at the peak wavelength. $R_m(\lambda_t)$ is calculated by using the known refractive index of the bottom layer.

4.2 Surface Normal Estimation

We estimate the surface normal of the thin film by using the characteristic strip expansion method proposed by Horn[20]. This method uses the monotonically increasing intensity and steepest ascent in the gradient space. As mentioned in previous section, the peak intensity monotonically increases. We find that the peak intensity corresponds to the gradient. We explain about the correspondence below.

In the image coordinate, an object point (x, y, z) is mapped to a pixel (u, v) , for which $u = x$ and $v = y$ under the orthographic projection. If the object surface z is represented as follows,

$$z = f(x, y) \quad (14)$$

, then the surface normal vector is defined by Eq. (15).

$$(p, q, -1) = \left[\frac{\delta f(x, y)}{\delta x}, \frac{\delta f(x, y)}{\delta y}, -1 \right] \quad (15)$$

, where p and q are the parameters of the surface normal. The quantity (p, q) is the gradient of (x, y) and is called the “gradient space”.

Normalizing Eq. (15) as 1, the z component of the surface normal becomes

$$z = \frac{1}{\sqrt{p^2 + q^2 + 1}} \quad (16)$$

This component is also equal to the cosine of the incident angle. Setting $x^2 + y^2 + z^2 = 1$, the existence domain of $f(p, q)$ is on the circumference defined as

Eq. (17).

$$p^2 + q^2 = \frac{1}{\cos^2 \theta_1} - 1 \quad (17)$$

By Eq. (17), the existence domain of gradients corresponds to the peak intensity. The peak intensity is determined uniquely by the incident angle. Also the existence domain is defined uniquely by the incident angle as shown in Eq. (17). This correspondence makes it able to apply the characteristics strip expansion method to the thin film objects.

We describe the estimation procedure with Fig. 4. Red arrows are steepest ascents in the peak intensity map. Purple arrows are steepest ascent in the gradient space.

1. Drawing contour lines by sampling the peak intensity per 0.1
2. Start from the pixel (x_1, y_1) in captured image which gradient (p_1, q_1) is known
3. Moving to the steepest ascent direction of (p_1, q_1) in captured image and determining (x_2, y_2) as the next pixel where intersect with contour line of the peak intensity
4. Moving to the steepest ascent direction of (x_1, y_1) in gradient space and determining (p_2, q_2) as the next gradient where intersect with contour line of the gradient
5. Repeating steps 3 and 4 until the whole surface normal is estimated

4.3 Refractive Index and Film Thickness Estimation

The refractive index and the film thickness are important optical parameters for reconstructing the appearance of thin film. We developed a more effective method for estimating these parameters.

By Snell's law, the optical path difference of Ep. (3) is rewritten as

$$\varphi = 2d\sqrt{n_2^2 - \sin^2 \theta_1} \quad (18)$$

The optical path difference becomes an integral multiple of the peak wavelength.

$$m\lambda_t = 2d\sqrt{n_2^2 - \sin^2 \theta_1} \quad (19)$$

, where m is a natural number. Using Eq. (19), the film thickness is defined as

$$d = \frac{m\lambda_t}{2\sqrt{n_2^2 - \sin^2 \theta_1}} \quad (20)$$

Therefore, we only need to check the combinations of the refractive index and the film thickness that fit the integral multiples of the peak wavelength. This enables us to reduce the computational time considerably, comparing with that required for the full search.

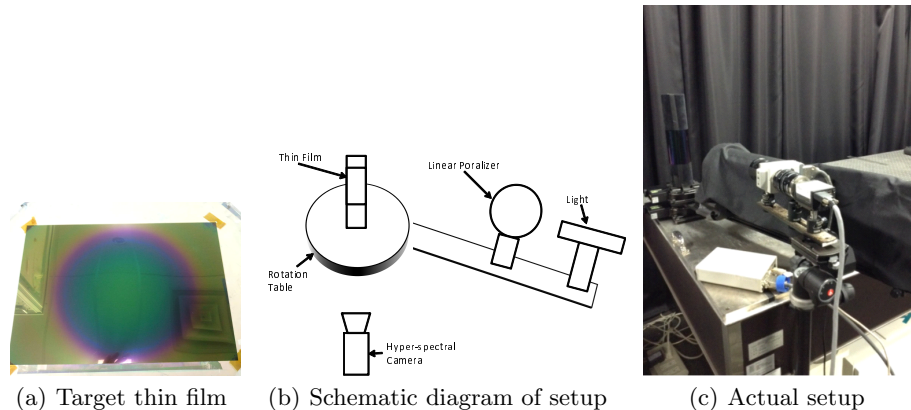


Fig. 5. Experimental setup for measuring thin film reflectance. (a) shows target thin film. (b) shows schematic diagram of setup. (c) shows actual setup. Distance between light source and the thin film was 0.8 m. Distance between the camera and the thin film was 0.6 m.

We determine the refractive index and film thickness by minimizing the square error between the reflectance model and the measured reflectance. The uniqueness of this minimization is guaranteed experimentally. Eq. (21) has some local minima, but it only has global minimum around ground truth.

$$\text{Arg min}_{n_2, m} \left| \sum_{\lambda} R_o(\lambda) - R_m(\lambda) \right|^2 \quad (21)$$

$R_o(\lambda)$ is measured reflectance spectra. $R_m(\lambda)$ is calculated by using the reflectance model in Section 3.

As mentioned in the previous section, the refractive index n_2 is lower than that of the bottom layer. Also, it is higher than 1.0 which is the refractive index in a vacuum. Kobayashi et al.[6] showed that when the refractive index error is approximately 0.01, the color difference of the BRDF becomes sufficiently small. We change the refractive index n_2 by 0.01 from 1.0 to the refractive index of the bottom layer. We then increased the natural number m until the film thickness is less than 1000 nm.

5 Evaluation

We evaluate the accuracy of our method by simulation and real data. For the simulation, we used hemispherical and cylindrical objects. We set the refractive index of thin film to 1.37 and that of the bottom layer to 1.6 which was the same as that of the real object. We set the film thickness to 400 nm for the hemispherical object and 420 nm to 560 nm along the x-axis for the cylindrical object.

Fig. 5 shows the setup for the thin film reflectance measurement to acquire the real data. A light source was attached to the rotation table to adjust the

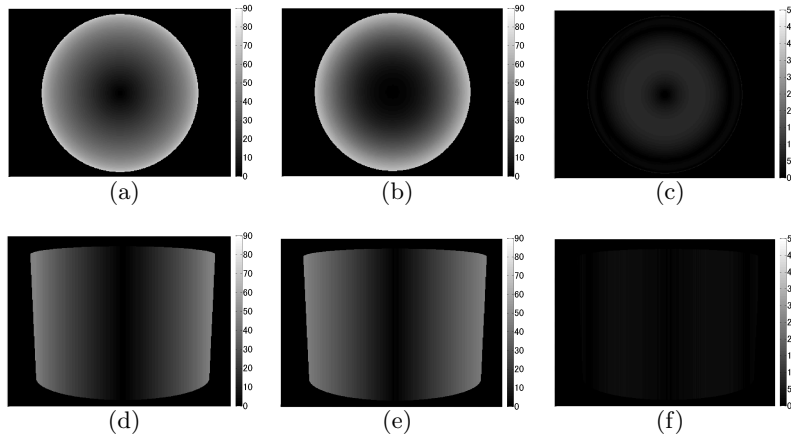


Fig. 6. Incident angle estimation results by simulation. (a) and (d) are ground truths. (b) and (e) are estimated results. (c) and (f) are estimation errors.

incident angle. The target thin film was MgF_2 which refractive index is 1.37. The film thickness was 400 nm. The refractive index of the bottom layer was 1.6, made of polyethylene terephthalate. We varied the incident angle from 10 to 42.5 degrees by 2.5 degrees.

The measurement device was a hyper-spectral camera, which consists of a liquid crystal tunable filter (Vari Spec CRI) and a monochrome camera. The liquid crystal tunable filter (LCTF) can change its transmitted wavelengths electrically. The viewing angle of the camera is approximately 30 degrees. The band width in this experiment was 4 nm. We putted a linear polarizer, which transmits S-wave. LCTF also transmits linearly polarized light, so we can capture S-wave reflectance. The transmittance of LCTF is only 4 % around 400 nm. The brightness of S-wave is stronger than that of P-wave, therefore we measure S-wave.

5.1 Incident Angle

Fig. 6 shows the incident angle estimation results of the simulation. Fig. 6 (b) and (e) show the estimated incident angles. Fig. 6 (c) and (f) show the estimation errors. The error increased around 0 to 20 degrees. The error of the spherical object is about 10 degree in this area. In other area, it becomes less than 3 degree. The error of the cylindrical object is about 5 degree in this area. In other are, it becomes less than 3 degree.

Fig. 7 shows the captured reflectance and the estimated result of the real data. The error also increased around 0 to 20 degrees. The error was approximately 9 degrees in this area. At other incident angles, the error was less than 5 degrees.

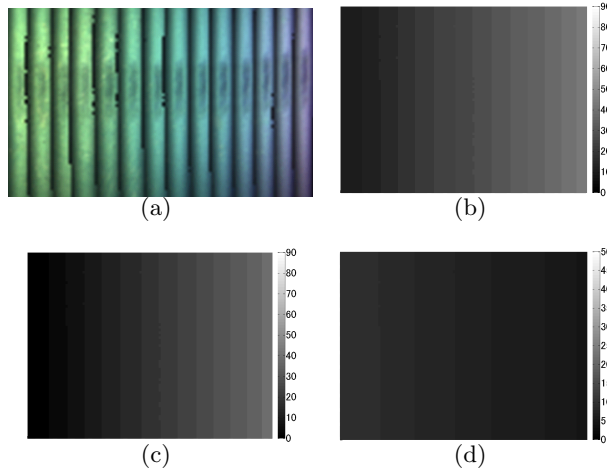


Fig. 7. Incident angle estimation results of real data. (a) shows input reflectance image. (b) shows ground truth incident angle. (c) shows estimated incident angle. (d) shows estimation error.

5.2 Surface Normal

By delimiting the estimated incident angle in Section 5.1 by 3 degrees, we estimated the surface normal by the characteristic strip expansion method. Fig. 8 (b) and (e) show the estimated results.

Fig. 8 (c) and (f) show the estimation errors. The estimation error was calculated as the angle between the ground truth normal and the estimated normal. The maximum error for the hemispherical object was approximately 10 degrees, and that of the cylinder was about 4 degrees. These errors include incident angle errors, then the error of surface normal estimation is about 1 degree. Therefore, the areas in which these errors occurred were the same as the areas where the incident angle errors were large.

5.3 Refractive Index and Film Thickness

We estimated the refractive index and film thickness, by using the estimated incident angle in Section 5.1. For the simulation, the estimated refractive index of the hemispherical and cylindrical objects was 1.37. Fig. 9 (b) and (e) show the estimated film thicknesses. Fig. 9 (c) and (f) show the estimation errors. The error of the hemispherical object was approximately 10 nm in the area where the error of the incident angle became larger. The error of cylindrical object was about 7 nm in the same area. For the real data, the estimated refractive index was 1.41. Fig. 10 (b) shows the estimated thickness. Fig. 10 (c) shows the estimation error. The average error was 45 nm.

We calculated the average color difference and root mean square error (RMSE) between the measured reflectance and the reflectance with estimated parameters.

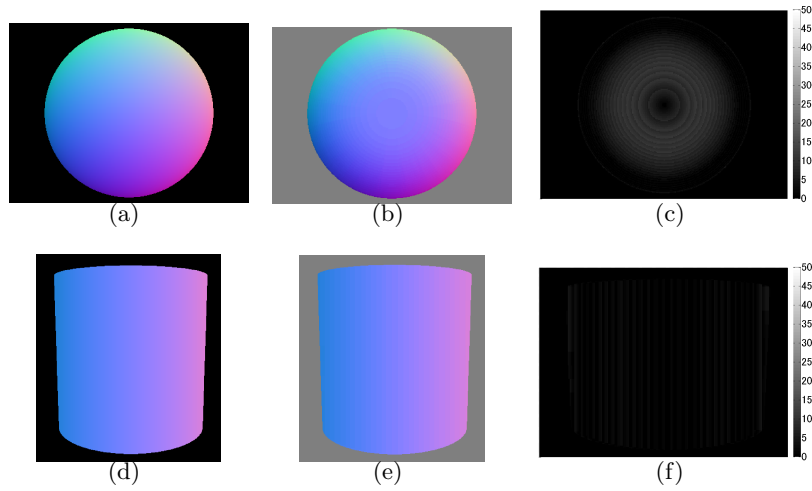


Fig. 8. Surface normal estimation results by simulation. (a) and (d) are ground truth. (b) and (e) are estimated normals. (c) and (f) are estimation errors.

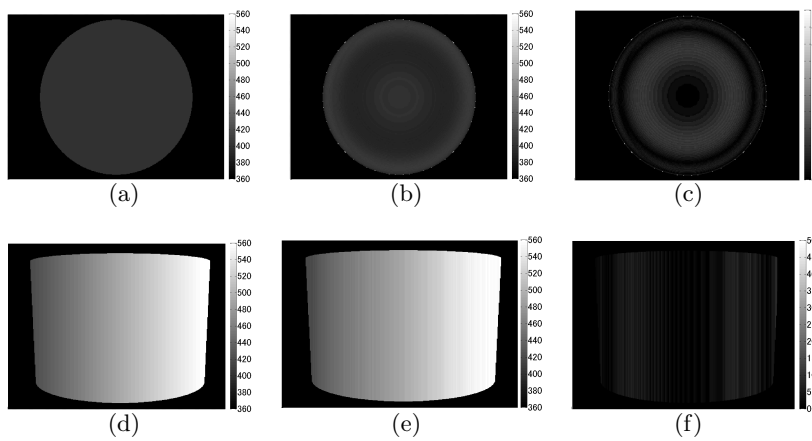


Fig. 9. Film thickness estimation results by simulation. (a) and (d) are ground truths. (b) and (e) are estimated results. (c) and (f) are estimation errors.

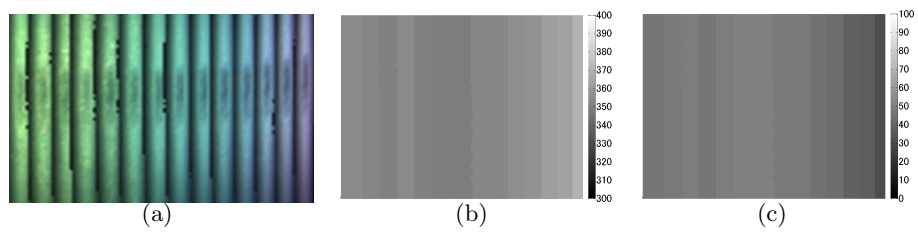


Fig. 10. Film thickness estimation result of real data. (a) shows input reflectance image. (b) shows estimated film thickness. (c) shows estimation error.

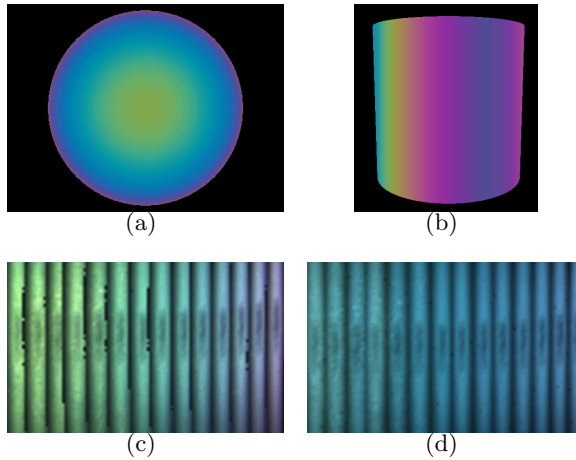


Fig. 11. Image synthesized with estimated surface normal, refractive index, and film thickness. (a) and (b) are results for simulation data. (c) is reflectance image by captured with the hyper-spectral camera. (d) is synthesized reflectance image for real data.

The color difference was calculated using Eq. (22).

$$\Delta E^*_{ab} = \sqrt{(\Delta L^*)^2 + (\Delta a^*)^2 + (\Delta b^*)^2} \quad (22)$$

The RMSE is defined as Eq. (23).

$$RMSE = \sqrt{(R_o(\lambda) - R_e(\lambda))^2 / N} \quad (23)$$

$R_o(\lambda)$ is the measured reflectance. $R_e(\lambda)$ is reflectance calculated by using the estimated parameters. The color difference was approximately 3.33, which can be perceived as a slight difference from the levels given in Table 1. The RMSE was about 2 % for each wavelength intensity.

Fig. 11 shows the rendering results with the estimated surface normal, refractive index and film thickness. Fig. 11 (a) and (b) are the reconstructed appearance of simulation data. Fig. 11 (c) is the image captured by using the hyper-spectral camera and (d) is the synthesized image.

6 Discussion

In this section, we discuss estimation results of the incident angle, surface normal, and optical parameters. The error of the incident angle became larger around 0 to 20 degrees. In these areas, the peak wavelengths were close to each other. This is very close to the sampling interval of the simulation data and the bandwidth of the hyper-spectral camera, so intensity detection became difficult. The error of the surface normal and optical parameters became large in the same area where the error of the incident angle became large. This error occurred because

Table 1. Level of difference or distance between two Colors

Level of color difference	ΔE^*_{ab}
trace	0 ~ 0.5
slight	0.5 ~ 1.5
noticeable	1.5 ~ 3.0
appreciable	3.0 ~ 6.0
great	6.0 ~ 12.0
very great	over 12.0

of the incident angle estimation error. The error of the optical parameters error of the real data becomes large outside these areas. The measured reflectance included noise which make the detection accuracy of the peak wavelength lower. Therefore, we can avoid these errors by using a high wavelength resolution and hyper-spectral camera with less noise.

Comparing the synthesized image Fig. 11 (d) and real image Fig. 11 (c), we can perceive the difference. The color difference occurs by the error of the incident angle and rounding error of captured reflectance spectra around 430 nm. Over 40 degree, the sample MgF_2 has the peak intensity around 430 nm, but hyper-spectral camera could not capture it with enough brightness because of its low transmittance. The low transmittance cause the rounding error which effects as noise, so we have the difference. The wavelength dependency of the refractive index is also considerable. However, we experimentally verified it does not effect to the estimated appearance for this sample.

We could estimate the incident angle and optical parameters even in darker areas in Fig. 11 (c). In darker areas, just the intensity of the measured reflectance is small, and we could measure reflectance spectra correctly. Therefore, estimated results of Fig. 7 (c) and 10 (b) had parameters in darker areas in Fig. 11 (c).

7 Conclusion

We proposed a novel method for estimating the shape and appearance of a thin film. We found that the peak intensity increased monotonically along incident angle, so we could use the characteristic strip expansion method to estimate the thin film surface normal. We also developed a more efficient method for estimating the refractive index and the film thickness by using the peak wavelength, where the optical path difference becomes an integral multiple of the peak wavelength. We conducted an experiment by simulation and real data and showed the effectiveness of our method. Our future work is to estimate more complicated shapes.

References

1. Iwasaki, K., Matsuzawa, K., Nishita, T.: Real-time rendering of soap bubbles taking into account light interference. In: Proceedings of the Computer Graphics International. CGI '04, Washington, DC, USA, IEEE Computer Society (2004) 344–348

2. Meinstner, K.W.: Interference spectroscopy. part i. *J. Opt. Soc. Am.* **31** (1941) 405–426
3. Azzam, R., Bashara, N.: *Ellipsometry and polarized light*. North-Holland personal library. North-Holland Pub. Co. (1977)
4. Kitagawa, K.: Thin-film thickness profile measurement by three-wavelength interference color analysis. *Appl. Opt.* **52** (2013) 1998–2007
5. Kitagawa, K.: Transparent film thickness measurement by three-wavelength interference method: An extended application of global model fitting algorithm. In: *Mechatronics (MECATRONICS)*, 2012 9th France-Japan 7th Europe-Asia Congress on and Research and Education in Mechatronics (REM), 2012 13th Int'l Workshop on. (2012) 94–100
6. Kobayashi, Y., Morimoto, T., Sato, I., Mukaigawa, Y., Ikeuchi, K.: Brdf estimation of structural color object by using hyper spectral image. In: *Computer Vision Workshops (ICCVW)*, 2013 IEEE International Conference on. (2013) 915–922
7. Scharstein, D., Szeliski, R.: A taxonomy and evaluation of dense two-frame stereo correspondence algorithms. *International Journal of Computer Vision* **47** (2002) 7–42
8. Herbot, S., Whaler, C.: An introduction to image-based 3d surface reconstruction and a survey of photometric stereo methods. *3D Research* **2** (2011)
9. Morris, N.J.W., et al.: Reconstructing the surface of inhomogeneous transparent scenes by scatter-trace photography (2007)
10. Oxholm, G., Nishino, K.: Shape and reflectance from natural illumination. In: *Fitzgibbon, A., Lazebnik, S., Perona, P., Sato, Y., Schmid, C., eds.: European Conference on Computer Vision. Volume 7572 of Lecture Notes in Computer Science*. Springer Berlin Heidelberg (2012) 528–541
11. Morimoto, T., Tan, R., Kawakami, R., Ikeuchi, K.: Estimating optical properties of layered surfaces using the spider model. In: *Computer Vision and Pattern Recognition (CVPR)*, 2010 IEEE Conference on. (2010) 207–214
12. Hirayama, H., Kaneda, K., Yamashita, H., Monden, Y.: An accurate illumination model for objects coated with multilayer films. *Computers and Graphics* **25** (2001) 391–400
13. Hirayama, H., Yamaji, Y., Kaneda, K., Yamashita, H., Monden, Y.: Rendering iridescent colors appearing on natural objects. In: *Computer Graphics and Applications, 2000. Proceedings. The Eighth Pacific Conference on*. (2000) 15–433
14. Sun, Y., Fracchia, F., Drew, M., Calvert, T.: Rendering iridescent colors of optical disks. In: *Rendering Techniques 2000. Eurographics*. Springer Vienna (2000) 341–352
15. Sun, Y., Fracchia, F.D., Calvert, T.W., Drew, M.S.: Deriving spectra from colors and rendering light interference. *IEEE Comput. Graph. Appl.* **19** (1999) 61–67
16. Sadeghi, I., Muñoz, A., Laven, P., Jarosz, W., Seron, F., Gutierrez, D., Jensen, H.W.: Physically-based simulation of rainbows. *ACM Transactions on Graphics (Presented at SIGGRAPH)* **31** (2012) 3:1–3:12
17. Cuypers, T., Haber, T., Bekaert, P., Oh, S.B., Raskar, R.: Reflectance model for diffraction. *ACM Trans. Graph.* **31** (2012) 122:1–122:11
18. Kinoshita, S.: *Structural Colors in the Realm of Nature*. World Scientific (2008)
19. L.S.Pedrotti: *Basic Physical Optics*. SPIE Press Book (2008)
20. Horn, B.K.: A problem in computer vision: Orienting silicon integrated circuit chips for lead bonding. *Computer Graphics and Image Processing* **4** (1975) 294 – 303